B. Boukhezzar
e-mail: boubekeur.boukhezzar@greyc.ensicaen.fr

H. Siguerdidjane
e-mail: houria.siguerdidjane@supelec.fr

Automatic Control Department,
Supélec,
Gif-sur-Yvette, F-91192
Cedex, France

M. Maureen Hand
National Renewable Energy Laboratory,
National Wind Technology Center,
1617 Cole Blvd., MS 3811,
Golden, CO 80401

Nonlinear Control of Variable-Speed Wind Turbines for Generator Torque Limiting and Power Optimization[1]

To maximize wind power extraction, a variable-speed wind turbine (VSWT) should operate as close as possible to its optimal power coefficient. The generator torque is used as a control input to improve wind energy capture by forcing the wind turbine (WT) to stay close to the maximum energy point. In general, current control techniques do not take into account the dynamical and stochastic aspect of both turbine and wind, leading to significant power losses. In addition, they are not robust with respect to disturbances. In order to address these weaknesses, a nonlinear approach, without wind speed measurement for VSWT control, is proposed. Nonlinear static and dynamic state feedback controllers with wind speed estimator are then derived. The controllers were tested with a WT simple mathematical model and are validated with an aeroelastic wind turbine simulator in the presence of disturbances and measurement noise. The results have shown better performance in comparison with existing controllers. [DOI: 10.1115/1.2356496]

1 Introduction

Variable-speed wind turbines have received a great deal of attention in recent years [1]. Structural loads can be reduced and energy capture increased with variable-speed operation. Also, the significant power excursions common to constant-speed turbines are avoided. However, sophisticated control algorithms are necessary for variable-speed wind turbines to be profitable and reliable.

Variable-speed wind turbines operate in two primary regimes, below-rated power and above-rated power. When power production is below the rated power for the machine, the turbine operates at variable rotor speeds to capture the maximum amount of energy available in the wind. Generator torque provides the control input to vary the rotor speed, and the blade pitch angle is held constant. At rated power, the primary objective is maintaining constant, rated power output. This is generally achieved by holding the generator torque constant and varying the blade pitch angle. In both control regimes, the turbine response to transient loads must be minimized. This study focuses on control algorithms designed for the below-rated power operating regime.

Several wind turbine controllers have been proposed for the variable-speed operating regime. Reference [2] defines the control objective as achieving optimal rotational speed tracking while rejecting fast wind speed variations and avoiding significant control efforts that induce undesirable torques and forces on the wind turbine structure. Several control strategies have been proposed in the literature primarily based on linear time-invariant (LTI) models. Classical controllers have also been used extensively. Optimal control has been applied in the linear quadratic (LQ) [3,4] and linear quadratic Gaussian (LQG) [4,5] forms. Robust control was introduced in Refs. [6,7]. More recently, some nonlinear control laws have been proposed [8], and adaptive control has also been studied [9]. However, as mentioned in Ref. [2], the drawbacks of these methods remain in the fact that nonlinear characteristics of the WT aerodynamics and structural behavior as well as the stochastic nature of the wind are not taken into consideration. In fact, by assuming the wind turbine operates in steady-state conditions, the dynamic equations governing the WT behavior are not considered. Also, these papers assume that the WT operates on its optimal power curve to simplify the control laws synthesis. Because of the variability in the wind, the WT deviates significantly from the optimal power curve. Consequently the assumption of steady-state operation is not valid. Many investigations also required a measurement of the wind speed, which is generally obtained with a single anemometer. This single-point measurement does not adequately describe the full-field turbulent inflow that impinges upon the rotor. Also, this signal is generally averaged, but the control law is based upon an instantaneous value.

The objective of this paper is to demonstrate the feasibility of robust nonlinear controllers that take into consideration the dynamic aspect of the wind speed variation and the wind turbine response without need of wind speed measurements. The following section provides a brief description of WT model requirements. A simplified mathematical model is derived, and a complicated aeroelastic simulation is described. The control objectives of this work are specified, and existing control techniques are summarized. Section 3 describes the aerodynamic torque and wind speed estimator used in the proposed nonlinear state feedback controllers. The estimated aerodynamic torque and wind speed are obtained from noisy measurements of the rotor speed and the generator torque. The nonlinear feedback controllers are presented in Sec. 4. The dynamic state feedback controller with asymptotic rotor speed reference tracking combined with the estimator is shown to meet the required specifications in spite of the presence of a constant disturbance and measurement noise. Finally, Sec. 5 compares the performance results of the nonlinear feedback controllers with other controllers in the literature.

2 Wind Turbine Modeling

2.1 Model Description. A wind turbine transforms part of the kinetic energy in the wind into electrical power. Wind turbine simulation complexity varies greatly depending upon its objectives. Aeroelastic simulators are used to verify dynamic loads and interaction of the components of these large flexible structures. The combination of aerodynamic loading and dynamic response of multiple components requires complex simulators. Many ef-

[1]This work has been carried out within the project Energie launched by Supélec.
Contributed by the Solar Energy Division of ASME for publication in the JOURNAL OF SOLAR ENERGY ENGINEERING. Manuscript received March 13, 2006; final manuscript received August 14, 2006. Review conducted by Panagiotis (Takis) Chaviaropoulos.

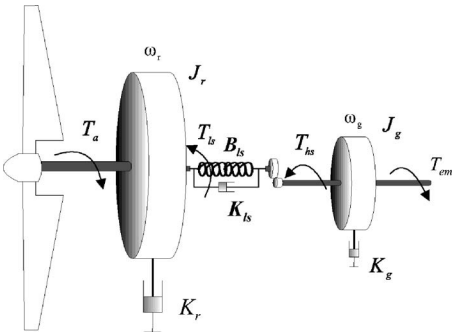

Fig. 1 Wind turbine dynamics

forts have been dedicated to the study of aeroelasticity and structural dynamics, and these efforts have produced wind turbine simulators that provide good predictions of loads and performance.

However, the complexity of such models is unnecessary for controller design. Consequently, simplified engineering models are developed for control design. These models are simpler and easier to manage. They are generally described by a set of nonlinear ordinary differential equations that describe limited degrees of freedom of the wind turbine. The aerodynamic loads in these models are generally computed with semi-empirical models. These simplified fluid flow dynamics may lead to inaccurate results under certain conditions, particularly near and beyond stall. The model simplicity depends on the controller objectives. In this work, a simplified mathematical model is used for control law synthesis in the aim of the wind turbine power/speed regulation. This model turns out to be sufficient for this purpose. However, one may need a more complex model for more controller objectives, as for example, this model should include the rotor flexibility when an individual pitch controller is used for rotor load alleviation [10,11].

Once the controllers are tested on the considered simplified mathematical model, a complex aeroelastic simulator is used for validation of the controller's performance.

2.2 System Modeling. A variable-speed wind turbine generally consists of an aeroturbine, a gearbox, and a generator, as shown in Fig. 1. The aerodynamic power captured by the rotor is given by the nonlinear expression

$$P_a = \frac{1}{2}\rho\pi R^2 C_p(\lambda,\beta)v^3 \tag{1}$$

where ω_r is the rotor speed, R is the rotor radius, and ρ is the air density.

The power extracted from the wind, P_a, is proportional to the cube of the wind speed v. The power coefficient, C_p, depends on the blade pitch angle, β, and the tip-speed ratio, λ, which is defined as the ratio between the linear blade tip speed and the wind speed v.

$$\lambda = \frac{\omega_r R}{v} \tag{2}$$

Thus, any change in the rotor speed or the wind speed induces change in the tip-speed ratio leading to power coefficient variation. In this way, the generated power is affected. The aerodynamic torque coefficient is related to the power coefficient as follows. Using the relationship

$$P_a = \omega_r T_a \tag{3}$$

the aerodynamic torque expression is then

$$T_a = \frac{1}{2}\rho\pi R^3 C_q(\lambda,\beta)v^2 \tag{4}$$

where

$$C_q(\lambda,\beta) = \frac{C_p(\lambda,\beta)}{\lambda}$$

Power and torque coefficient surfaces for the wind turbine considered in this study are shown in Fig. 2. These surfaces are obtained using blade-element moment theory implemented in a wind turbine performance code, WT-PERF [12], developed by NREL. These surfaces are implemented in the mathematical model as look-up tables.

The dynamic response of the rotor driven at a speed ω_r by the aerodynamic torque T_a is shown to be

$$J_r\dot{\omega}_r = T_a - T_{ls} - K_r\omega_r \tag{5}$$

The low-speed shaft torque T_{ls} acts as braking torque on the rotor (see Fig. 1). It results from the torsion and friction effects due to the difference between ω_r and ω_{ls}

$$T_{ls} = B_{ls}(\dot{\theta}_r - \dot{\theta}_{ls}) + K_{ls}(\omega_r - \omega_{ls}) \tag{6}$$

The generator is driven by the high-speed shaft torque T_{hs} and braked by the generator electromagnetic torque T_{em}.

$$J_g\dot{\omega}_g = T_{hs} - K_g\omega_g - T_{em} \tag{7}$$

Assuming an ideal gearbox with transmission ratio n_g, we have

$$n_g = \frac{T_{ls}}{T_{hs}} = \frac{\omega_g}{\omega_{ls}} \tag{8}$$

Transferring the generator dynamics to the low-speed side and using Eqs. (7) and (8), the generator dynamics can be written as

$$n_g^2 J_g\dot{\omega}_g = T_{ls} - (n_g^2 K_g)\omega_g - n_g T_{em} \tag{9}$$

If a perfectly rigid low-speed shaft is assumed, a single mass model of the turbine may then be considered

$$J_t\dot{\omega}_r = T_a - K_t\omega_r - T_g \tag{10}$$

where

$$J_t = J_r + n_g^2 J_g$$

$$K_t = K_r + n_g^2 K_g$$

$$T_g = n_g T_{em}$$

2.3 Simulator Description. The Fatigue, Aerodynamics, Structures and Turbulence (FAST) code developed by NREL is an aeroelastic WT simulator that is capable of modeling two- and three-bladed propeller-type machines. This code is used by WT designers to predict both extreme and fatigue loads. It uses an assumed mode method to model flexible blades and tower components. Other components are modeled as rigid bodies. In this study, three degrees of freedom (DOFs) are simulated: the variable generator and rotor speed (2 DOFs) and the blade teeter DOF. The variable generator and rotor speed DOFs account for the variations in generator speed and the drive train flexibility associated with torsional motion between the generator and hub/rotor. The blade teetering DOF accounts for the teeter motion induced by asymmetric wind loads across the rotor plane.

2.4 Control Objectives. The $C_p(\lambda,\beta)$ curve in Eq. (1) is specific for each wind turbine. It has a unique maximum $C_{p_{opt}}$ at a single point

$$C_p(\lambda_{opt},\beta_{opt}) = C_{p_{opt}} \tag{11}$$

that corresponds to maximum power production in below-rated power conditions. To maximize wind power extraction, the blade pitch angle, β, is fixed to the optimal value, β_{opt}, and the WT

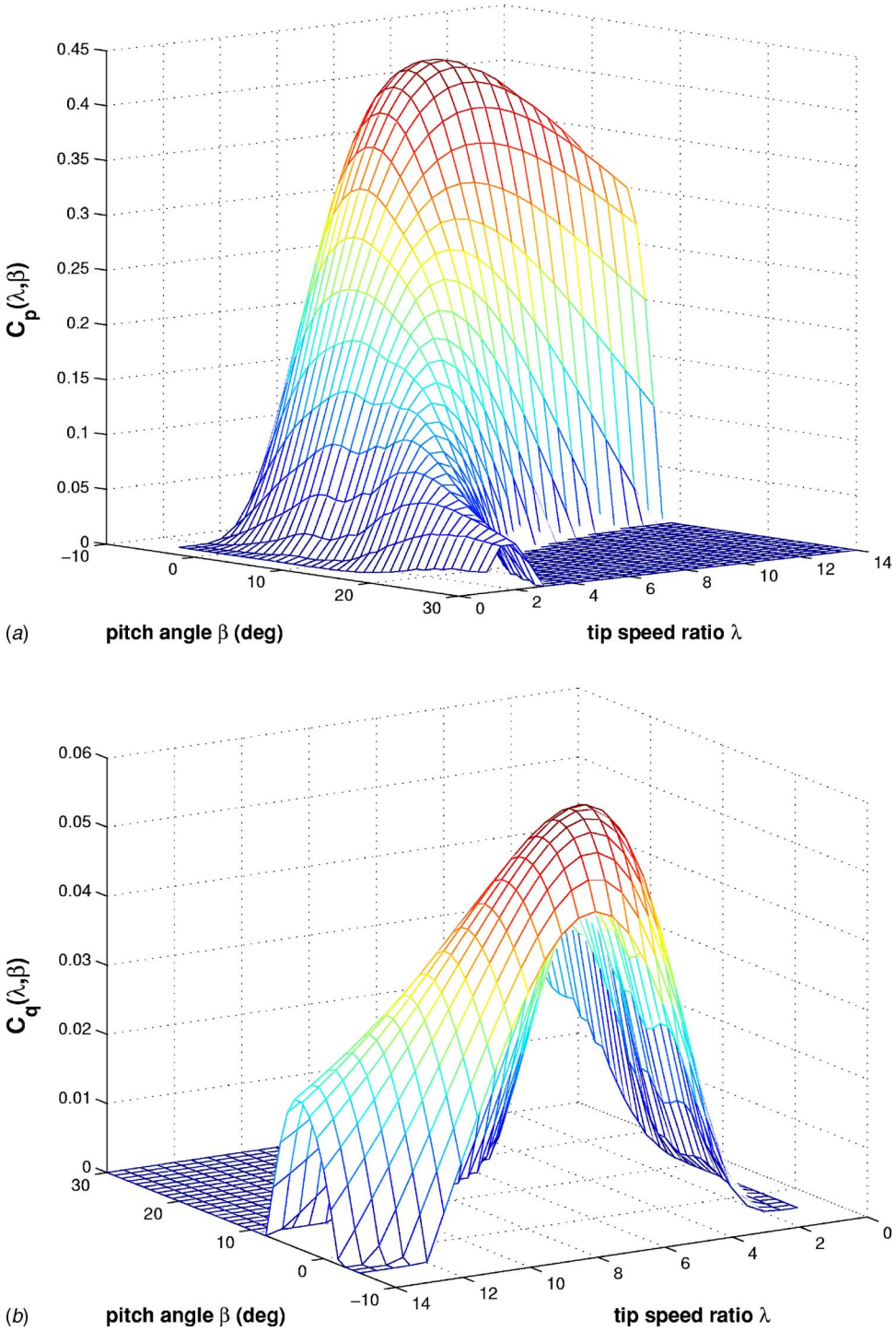

Fig. 2 Aerodynamic power and torque coefficients curves

should continuously operate at the optimal tip-speed ratio, λ_{opt}. For a given wind speed, v, in order to maintain λ at its optimal value, the rotor speed must be adjusted using generator torque to track the reference $\omega_{r_{opt}}$ that has the same shape as wind speed, since they are proportional.

$$\omega_{r_{opt}} = \frac{\lambda_{opt}}{R} v \tag{12}$$

Hence, in the partial load area, the WT is a single-input, single-output (SISO) system. The control input is the generator torque referenced to the low-speed side of the gearbox. The system output to be controlled is the rotor speed, ω_r, and the control problem is the tracking of an optimal rotor speed reference, $\omega_{r_{opt}}$, that ensures maximum wind power capture.

The low-speed shaft is selected to assess the effect of the controllers on the mechanical loads. This is due to many reasons: first, the drive train bearing failures occur more frequently than damages occurring on the other components as the tower or the rotor. Also, we assumed that the drive train loads on the dynamic characteristics of the assembled wind turbine are decoupled from the other turbine parts, in order to reduce the complexity of the numerical models. In addition, the load amplifications within the

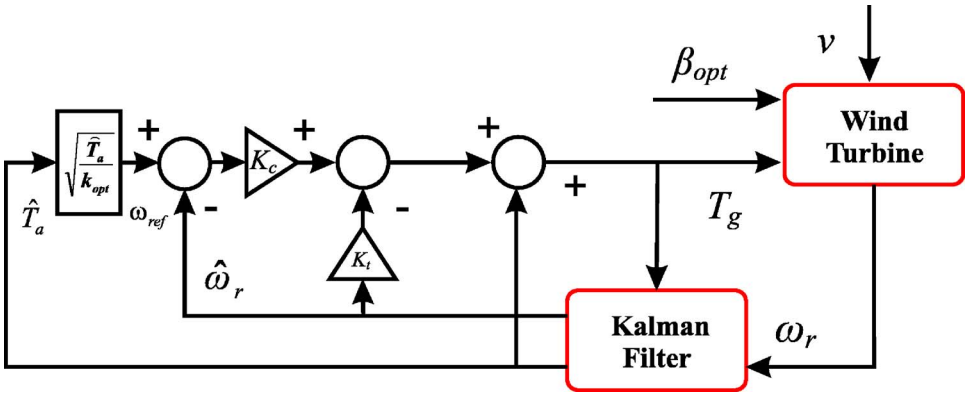

Fig. 3 ATF control scheme

gearbox are generally much larger than the amplifications that would be detected by experimental measurements or numerical simulations in the other turbine parts [13].

2.5 Baseline Control Strategies. In order to make a comparison between the proposed controllers and existing controllers, a brief description of two well-known control techniques is given here. In Ref. [14], an Aerodynamic Torque Feed Forward (ATF) controller is described. The aerodynamic torque and the rotor speed are estimated using a Kalman filter. The estimated aerodynamic torque is fed into the generator reference torque. A proportional control law is used.

$$T_g = K_c(\omega_{ref} - \hat{\omega}_r) + \hat{T}_a - K_t\hat{\omega}_r \tag{13}$$

where

$$\omega_{ref} = \sqrt{\frac{\hat{T}_a}{k_{opt}}} \tag{14}$$

with

$$k_{opt} = \frac{\rho}{2}\pi R^5 C_{p_{opt}} \frac{1}{\lambda_{opt}^3}$$

The control scheme is shown in Fig. 3.

In duplicating the ATF model for this study, from simulation results, a wind speed step response has shown a steady-state error, particularly in the presence of disturbances. The values of k_{opt} and $C_{p_{opt}}$ are generally obtained by the control engineer from performance models such as those used to determine the surfaces in Fig. 2. Since k_{opt} is proportional to $C_{p_{opt}}$, then, when the considered k_{opt} value is different from the turbine's real one, therefore, steady-state error will occur in this case [15]. It is worthwhile to mention that the problem with uncertainty of $C_{p_{opt}}$ has not been considered in this work. Nevertheless, it is quite important for experimentation on real machines. An additional drawback of this technique is the assumption that the WT operates close to the optimal rotor speed, ω_{ref}, which is obtained by setting $T_a = T_{a_{opt}}$. The difference between $\omega_{r_{opt}}$ and ω_{ref} induces significant power losses during the transitions. Therefore, a more precise value of ω_{ref} is needed.

It is shown in Ref. [16] that, under some specific conditions, by means of constant generator torque and wind speed, the wind turbine remains locally stable about any equilibrium point on the optimal aerodynamic efficiency curve. One can maintain T_a on this curve by choosing a control torque T_g that tracks the same value rather than tracking wind speed variations

$$T_g = k_{opt}\omega_r^2 - K_t\omega_r \tag{15}$$

This method is known as the indirect speed control (ISC) technique. Figure 4 shows the ISC control scheme. In constant wind speeds, the ISC controller will achieve the tip-speed ratio for optimum operation. However, in varying wind, the inertia of the rotor prevents continuous operation at $C_{p_{opt}}$ [17]. Nevertheless, the transitions during fast wind speed variations result in power losses. Additionally, the control strategy is not robust with respect to measurement noise and disturbances.

In summary, the control techniques described above show two main drawbacks: on the one hand, they do not take into consideration the dynamic aspect of the wind and the turbine; on the other hand, they are not robust with respect to measurement noise and disturbances. In order to address these weaknesses, a nonlinear dynamic state feedback controller with a wind speed estimator will be presented. Furthermore, this structure allows the rejection of disturbances acting on the control torque T_g.

3 Estimation of Wind Speed and Aerodynamic Torque

The wind speed, v, that appears in the aerodynamic torque and power expression of Eqs. (1) and (4) is actually a kind of spatial average of the three-dimensional wind speed field that impinges upon the rotor blades. This field varies over the disc swept by the rotor [18], it is then impossible to represent it by a unique measure. In practice, the wind speed measured by an anemometer does not represent the effective wind speed v. The rotor effective wind speed is defined as a single point wind speed signal, which will cause torque variations through thrust and torque coefficients that will be stochastically equivalent to those calculated with blade element theory in a turbulent wind field [19]. Aiming to obtain a more representative value of v and to control the wind turbine without using an anemometer signal, we use the wind turbine as a measurement device. We do this in two steps: estimation of the aerodynamic torque and deduction of the wind speed.

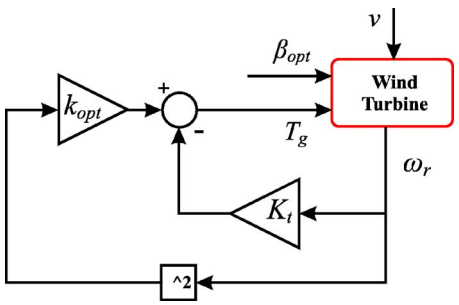

Fig. 4 ISC control scheme

3.1 Aerodynamic Torque Estimation. A Kalman filter is used to estimate aerodynamic torque T_a by appending it as an additional state. The dynamics for this state are driven by white noise

$$\begin{bmatrix} \dot{\omega}_r \\ \dot{T}_a \end{bmatrix} = \begin{bmatrix} -\frac{K_t}{J_t} & \frac{1}{J_t} \\ 0 & 0 \end{bmatrix} \begin{bmatrix} \omega_r \\ T_a \end{bmatrix} + \begin{bmatrix} -\frac{1}{J_t} \\ 0 \end{bmatrix} T_g + \begin{bmatrix} 0 \\ 1 \end{bmatrix} \xi$$

$$y = \omega_r + \zeta \tag{16}$$

ξ is the process noise and ζ the measurement noise. They are a centered white, noncorrelated, Gaussian noise. Reference [20] proves that if the state noise variance is nonzero, the Kalman estimator corresponding to the system in Eq. (16) is convergent. In this Kalman filter approach, the estimated state is not exploited to deduce the optimal reference speed $\omega_{r_{opt}}$. Rather, the estimated state $[\hat{\omega}_r, \hat{T}_a]^t$ is used to obtain an estimate of the effective wind speed, $\hat{v}$, from which the optimal rotor speed is derived. Besides, as the rotor speed measurement contains noise disturbances, it is preferable to use its estimate in the control laws.

3.2 Wind Speed Estimation. The aerodynamic torque depends nonlinearly on the rotor speed ω_r and also on the wind speed v. The effective wind speed v is related to T_a through the expression for aerodynamic torque when the pitch angle is held at its optimal value.

$$T_a = \frac{1}{2}\rho\pi R^3 C_q(\lambda) v^2 \tag{17}$$

where

$$C_q(\lambda) = C_q(\lambda, \beta_{opt})$$

Using Eq. (17) and the estimated aerodynamic torque and rotor speed obtained in Eq. (16), the estimate of wind speed, $\hat{v}$, is found by solving the following algebraic equation.

$$\hat{T}_a - \frac{1}{2}\rho\pi R^3 C_q\left(\frac{\hat{\omega}_r R}{\hat{v}}\right)\hat{v}^2 = 0 \tag{18}$$

In order to use numerical algorithms for solving Eq. (18), an analytic expression of $C_q(\lambda)$ is needed. Because it is given through a look-up table, C_q is approximated by a polynomial in λ.

$$C_q(\lambda) = \sum_{i=0}^{n} a_i \lambda^i$$

Equation (18) is finally solved using the Newton algorithm. Because this equation has a unique solution in the below rated power operating regime, the convergence of the algorithms is achieved after only a few iterations. Having $\hat{v}$, the estimated optimal rotor speed, $\hat{\omega}_{r_{opt}}$ is thus

$$\hat{\omega}_{r_{opt}} = \frac{\lambda_{opt}\hat{v}}{R} \tag{19}$$

It is important to note that estimation of $\omega_{r_{opt}}$ does require a good estimate of the wind speed. This estimator is then used to design nonlinear control laws for optimal rotor speed tracking of $\omega_{r_{opt}}$ to improve the aerodynamic efficiency while reducing the drive train transient loads.

4 Nonlinear State Feedback Control With Estimator

4.1 Nonlinear Static State Feedback Control With Estimator. The nonlinear behavior of the WT described by Eq. (10) is linearized using the aerodynamic torque estimate $\hat{T}_a$.

By imposing the following control torque,

$$T_g = J_t\left(\frac{\hat{T}_a}{J_t} - \frac{K_t}{J_t}\omega_r - w\right) \tag{20}$$

w is the new input of the linearized system. Equation (10) simplifies to

$$\dot{\omega}_r = w \tag{21}$$

A first-order dynamic response is selected for the rotor speed tracking error $\hat{\varepsilon}$.

$$\dot{\hat{\varepsilon}} + a_0\hat{\varepsilon} = 0, \quad a_0 > 0 \tag{22}$$

where

$$\hat{\varepsilon} = \hat{\omega}_{opt} - \hat{\omega}_r \tag{23}$$

From Eqs. (21) and (22), the new input w is obtained

$$w = \dot{\hat{\omega}}_{r_{opt}} + a_0(\hat{\omega}_{r_{opt}} - \hat{\omega}_r) \tag{24}$$

By substituting Eq. (24) of w in (20), the generator torque T_g is thus

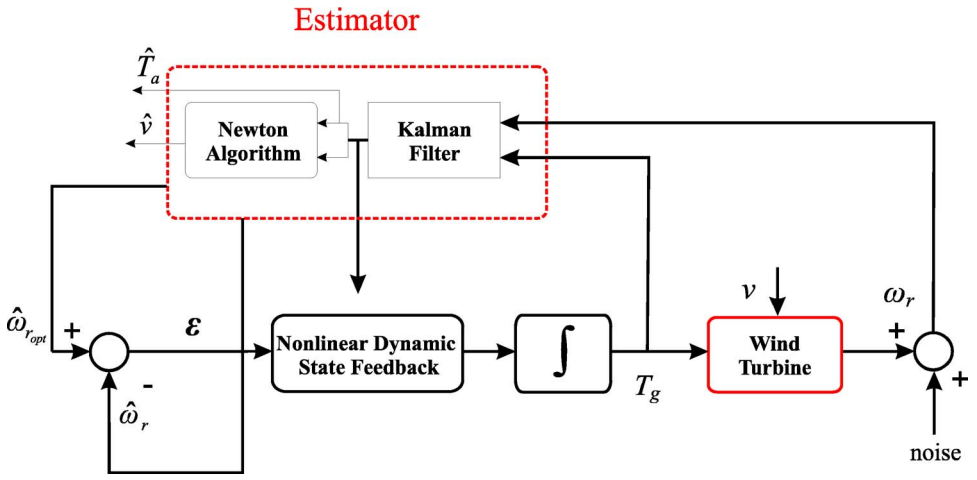

Fig. 5 Nonlinear dynamic state feedback with estimator controller scheme

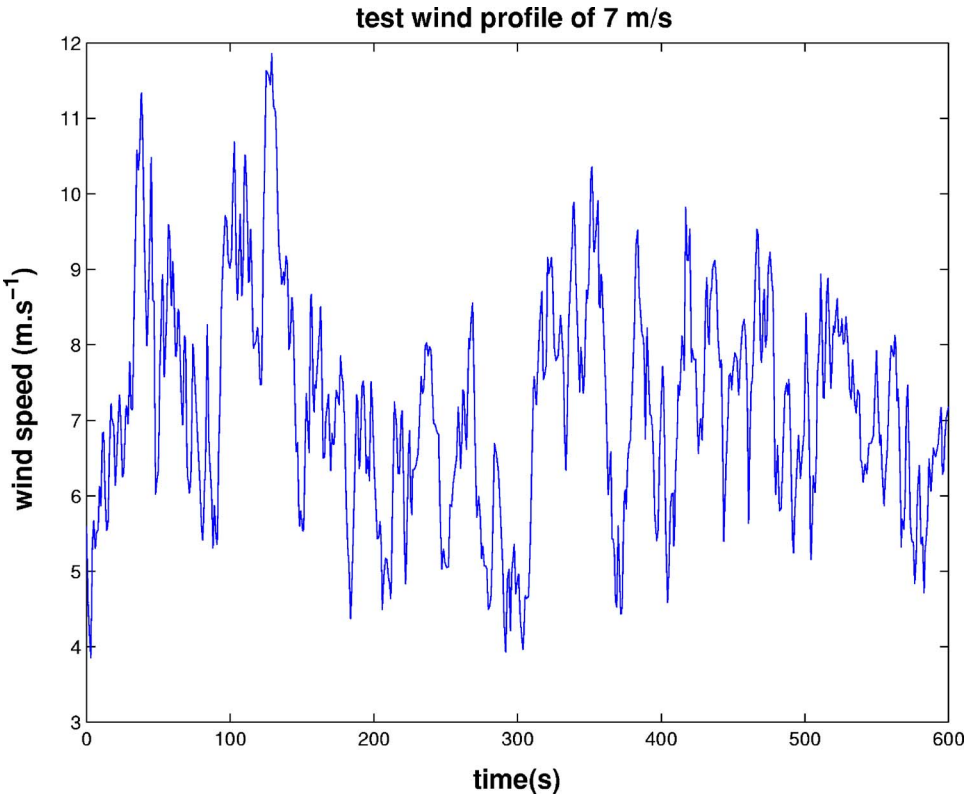

Fig. 6 Wind speed profile of 7 m·s^{-1} mean value

$$T_g = \hat{T}_a - K_t\hat{\omega}_r - J_t a_0\hat{\varepsilon} - J_t\dot{\hat{\omega}}_{t_{opt}} \tag{25}$$

This technique has been shown to lack robustness with respect to perturbations [21], so a nonlinear dynamic state feedback controller is developed next.

4.2 Nonlinear Dynamic State Feedback Control With Estimator. Higher order dynamic response of the tracking error can be imposed to produce a dynamic state feedback controller. Assuming a constant disturbance d acting on the wind turbine, Eq. (10) becomes

$$J_t\dot{\omega}_r = T_a - K_t\omega_r - T_g + d \tag{26}$$

The disturbance may represent an unmodeled or unknown phenomenon which affects the WT behavior, e.g., solid friction. Taking the time derivative of Eq. (26), we get

$$J_t\ddot{\omega}_r = \dot{T}_a - K_t\dot{\omega}_r - \dot{T}_g \tag{27}$$

As in the nonlinear static state feedback controller, the control torque

$$\dot{T}_g = \frac{1}{J_t}\left(\frac{\dot{\hat{T}}_a}{J_t} - \frac{K_t}{J_t}\dot{\hat{\omega}}_r - w\right) \tag{28}$$

results in a linear system with a new input, w. Substituting Eq. (28) into Eq. (10) results in

$$\ddot{\omega}_r = w \tag{29}$$

We now choose a second-order differential equation to govern the tracking error $\hat{\varepsilon}$

$$\ddot{\hat{\varepsilon}} + b_1\dot{\hat{\varepsilon}} + b_0\hat{\varepsilon} = 0; \tag{30}$$

the parameters b_0, b_1 are chosen in such a way that the polynomial $s^2+b_1s+b_0$ is Hurwitz (s indicates Laplace variable).

Substituting Eqs. (23) and (29) into Eq. (30) produces

$$w = \ddot{\hat{\omega}}_{r_{opt}} + b_1(\dot{\hat{\omega}}_{r_{opt}} - \dot{\hat{\omega}}_r) + b_0(\hat{\omega}_{r_{opt}} - \hat{\omega}_r) \tag{31}$$

and finally the generator torque dynamics are given by

$$\dot{T}_g = \dot{\hat{T}}_a - K_t\dot{\hat{\omega}}_r - J_t\ddot{\hat{\omega}}_{opt} - J_t b_1\dot{\hat{\varepsilon}} - J_t b_0\hat{\varepsilon} \tag{32}$$

A diagram of the dynamic state feedback controller with wind speed estimator is shown in Fig. 5. All the time derivatives that appear in the generator torque expressions, Eq. (25) and (32), are obtained using approximated filtered derivatives. Very fast dynamics will lead to wind speed turbulence tracking, but large control loads will also occur. So the dynamic response must be designed to track the average wind speed over short time intervals. This decreases the rapid variations in generator torque, which is beneficial. Very fast changes in T_g are not desirable. These objectives are performed by choosing appropriate dynamics for the tracking error. This choice will lead to slow the rotor speed and the generator torque variations resulting in smoothed output power.

The robustness of the controllers with regards to parameters variation is not considered in this study. An adaptive approach to take into consideration the parameters changes is proposed in [22] for a different controller structure. The robustification of the proposed controllers is planned to be presented in some future research work.

Table 1 Wind turbine characteristics

Rotor diameter	43.3 m
Gearbox ratio	43.165
Hub height	36.6 m
Generator system electrical power	600 kW
Maximum rotor torque	162 KN·m

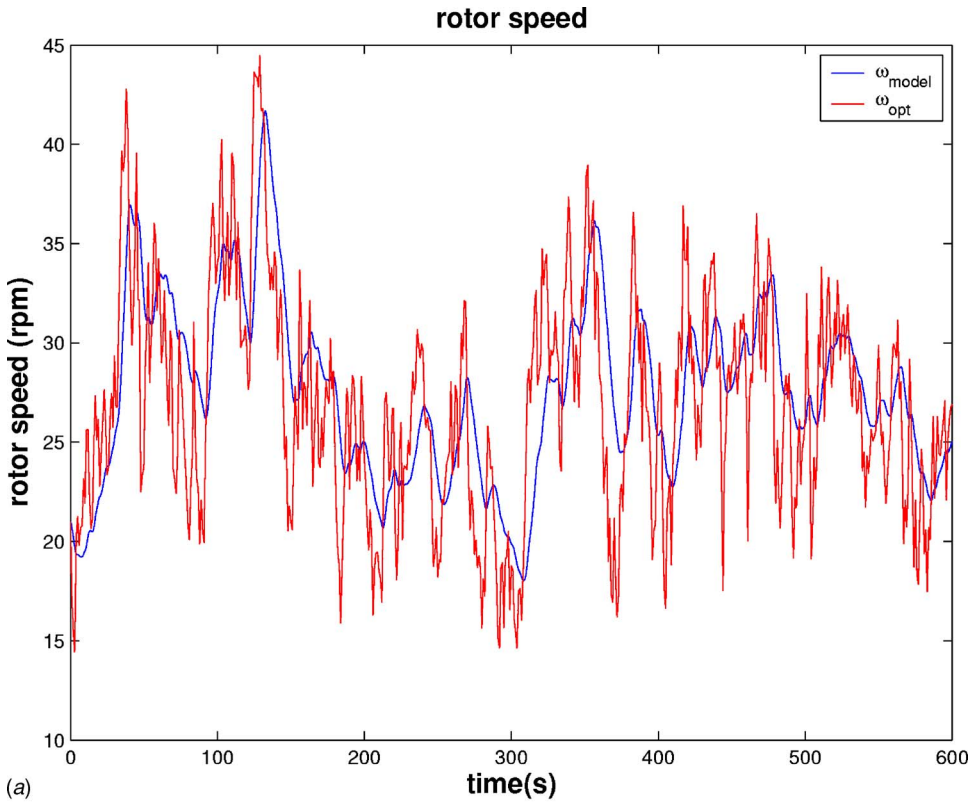

(*a*)

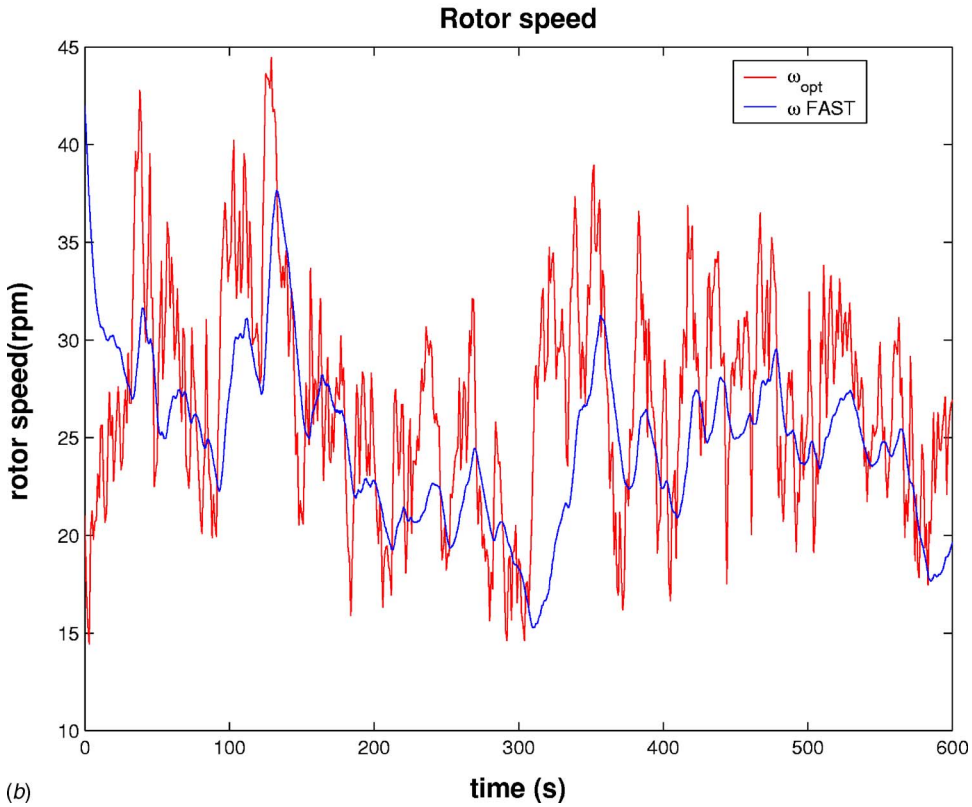

(*b*)

Fig. 7 Nonlinear dynamic state feedback control, with estimator: rotor speed responses

5 Validation Results

The numerical simulations were performed on a wind turbine whose characteristics are given in Table 1. These parameters correspond to the Controls Advanced Research Turbine (CART), which is located at NREL's National Wind Technology Center near Boulder, CO. The CART is a variable-speed, variable-pitch WT with a nominal power rating of 600 kW and a hub height of 36 m. It is a 43 m diameter, two-bladed, teetered hub machine.

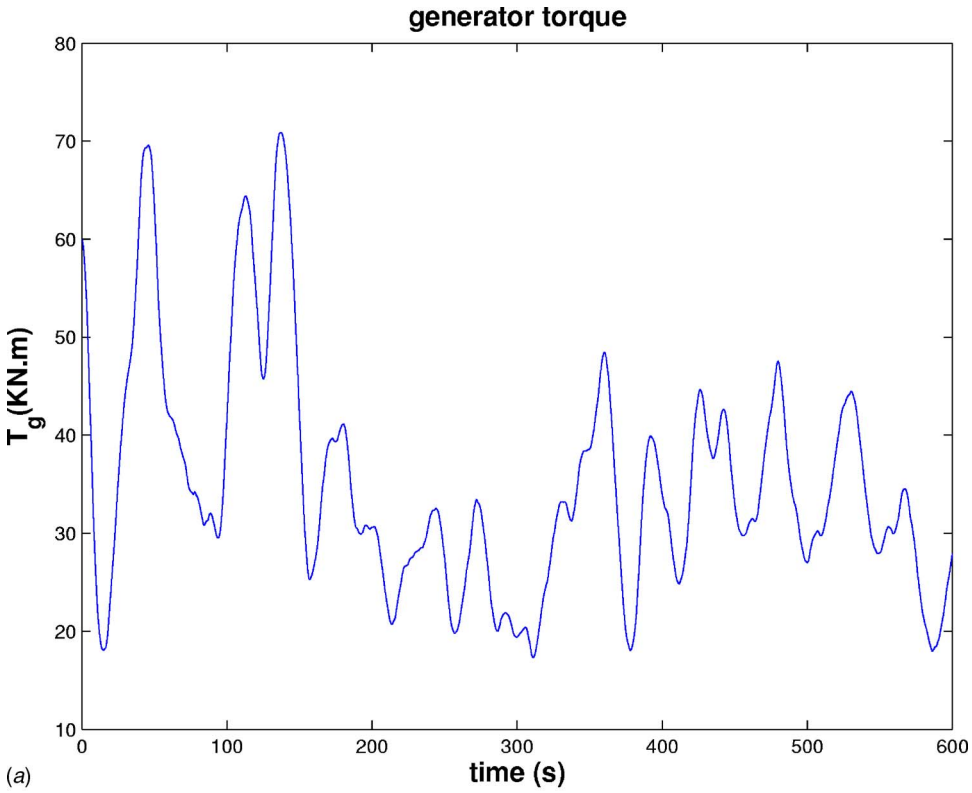

(*a*)

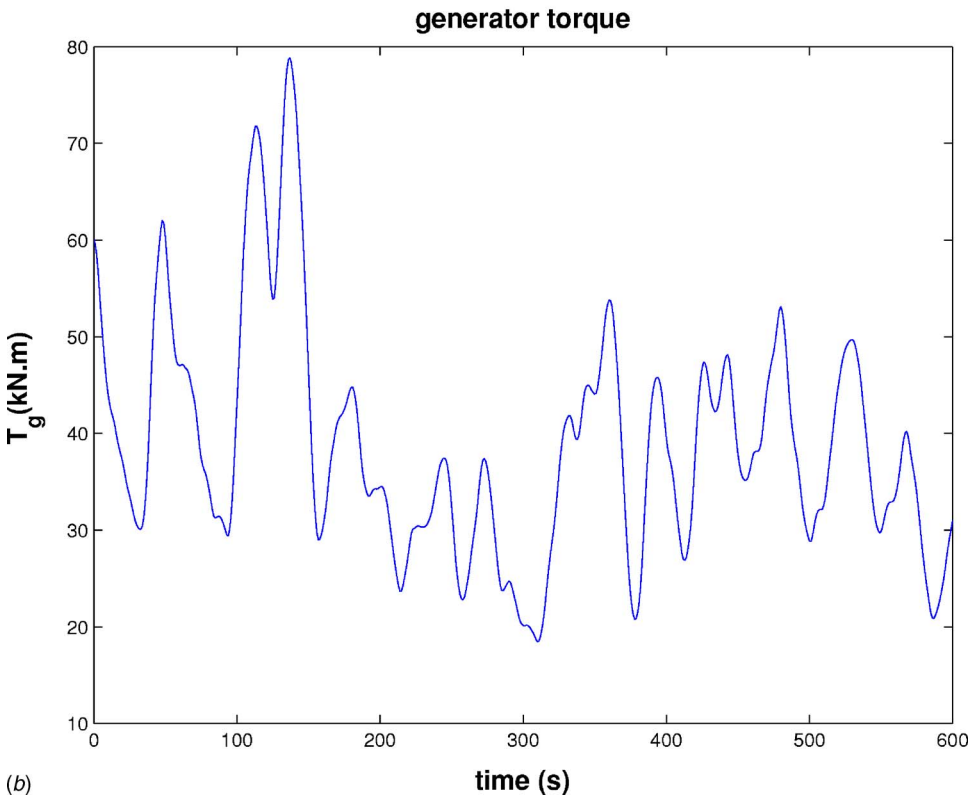

(*b*)

Fig. 8 Nonlinear dynamic state feedback control, with estimator: generator torque responses

The gearbox is connected to an induction generator via the high-speed shaft, and the generator is connected to the grid via power electronics. This turbine was modeled with the mathematical model and the FAST aeroelastic simulator for comparison.

The wind inflow for the simulations consists of a set of full-field turbulent wind.

Figure 6 illustrates the hub-height wind speed variation.

The instantaneous point wind speed v is the sum of two components such as:

$$v = v_m + v_t \tag{33}$$

where v_m is the mean value and v_t is the turbulent component.

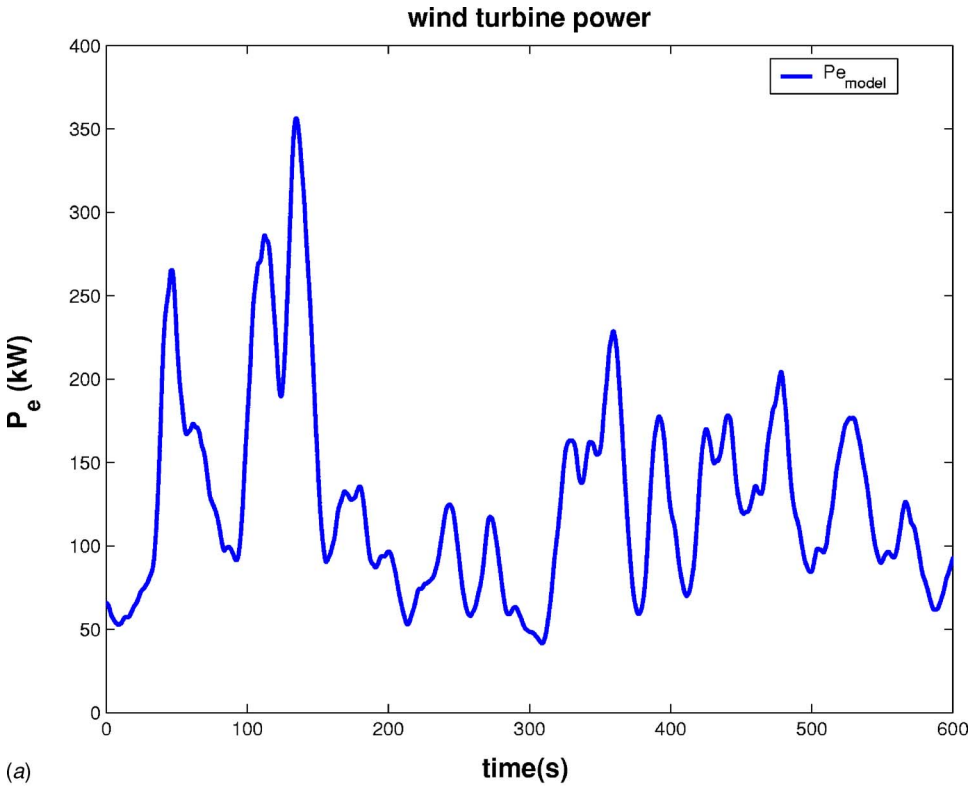

(*a*)

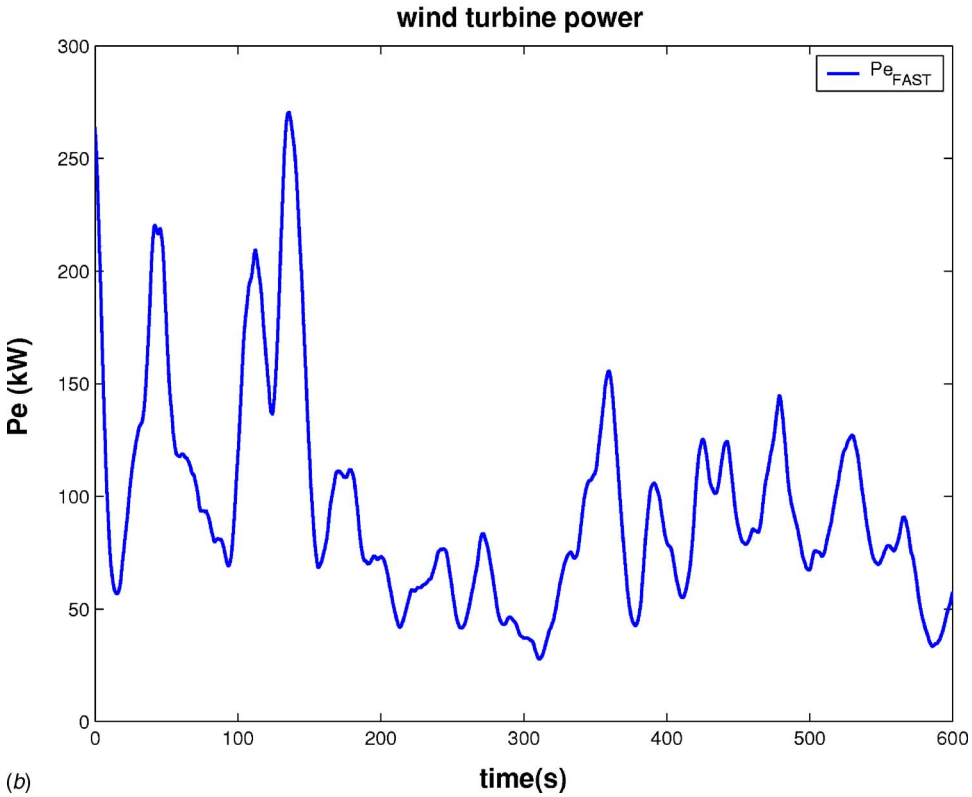

(*b*)

Fig. 9 Nonlinear dynamic state feedback controller, with estimator: wind turbine power

The Van der Hooven experimental wind spectra show that the mean value v_m has a peak at a period corresponding to 10 min on average [1]. For this purpose, a 10 min wind data set is chosen to keep a constant mean value.

This turbulent wind data were generated using the class A Kaimal turbulence spectra [4]. It has a mean value of 7 m/s at the hub height and a turbulence intensity of 25%. Using this excitation, each of the four controllers discussed is compared for energy capture and transient load reduction.

As mentioned in Sec. 2.4, the control objective is to maximize

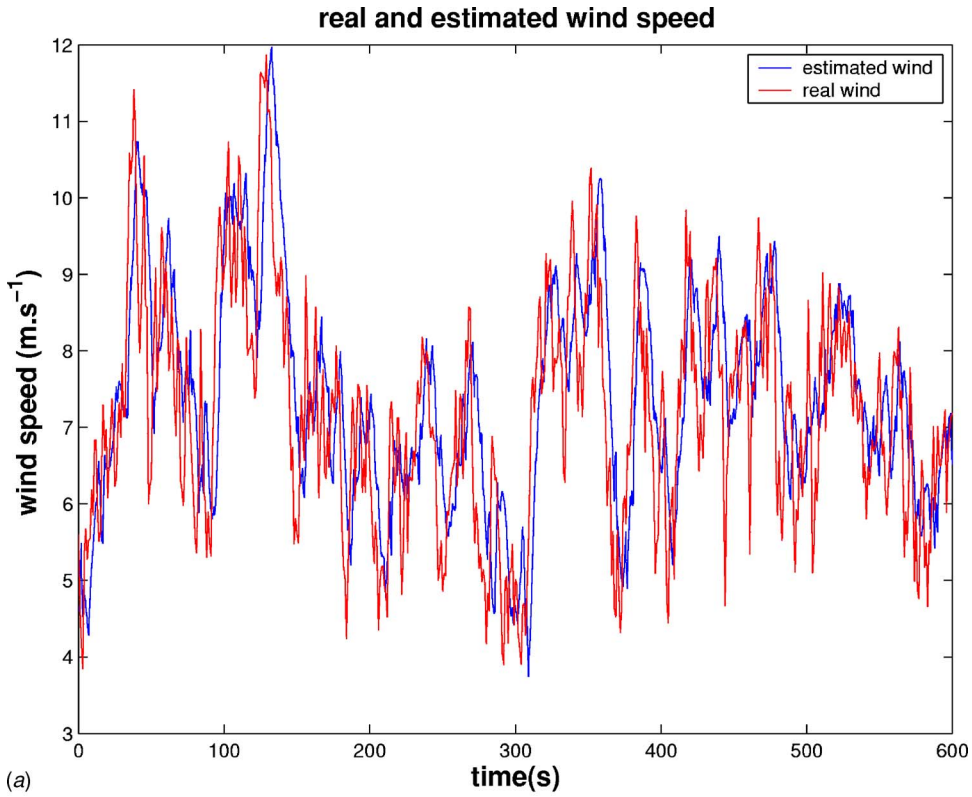

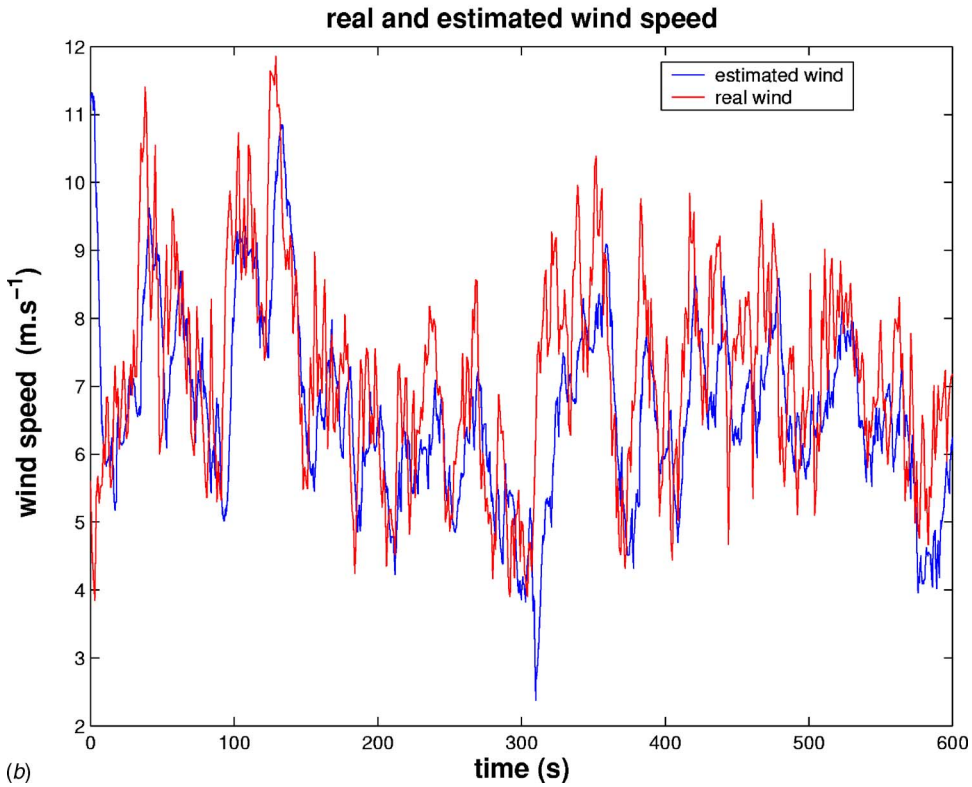

Fig. 10 Wind speed estimation

the captured energy from the wind while limiting the transient loads experienced by the turbine. For this study, the low-speed shaft torsion was minimized, which is equivalent to reducing the variance of the high-speed shaft torsional moment. It is observed that the generator torque and the rotor speed are both within the required constraints of 162 kN·m and 58 rpm [23], respectively.

5.1 Using the Simplified Mathematical Model. First, the performance of the nonlinear dynamic state feedback controller (5) is verified using the simplified mathematical model. An additive measurement noise on ω_r has been introduced. This is a band-limited, white noise obtained by using a normally distributed random number generator in series with a zeroth-order hold. This

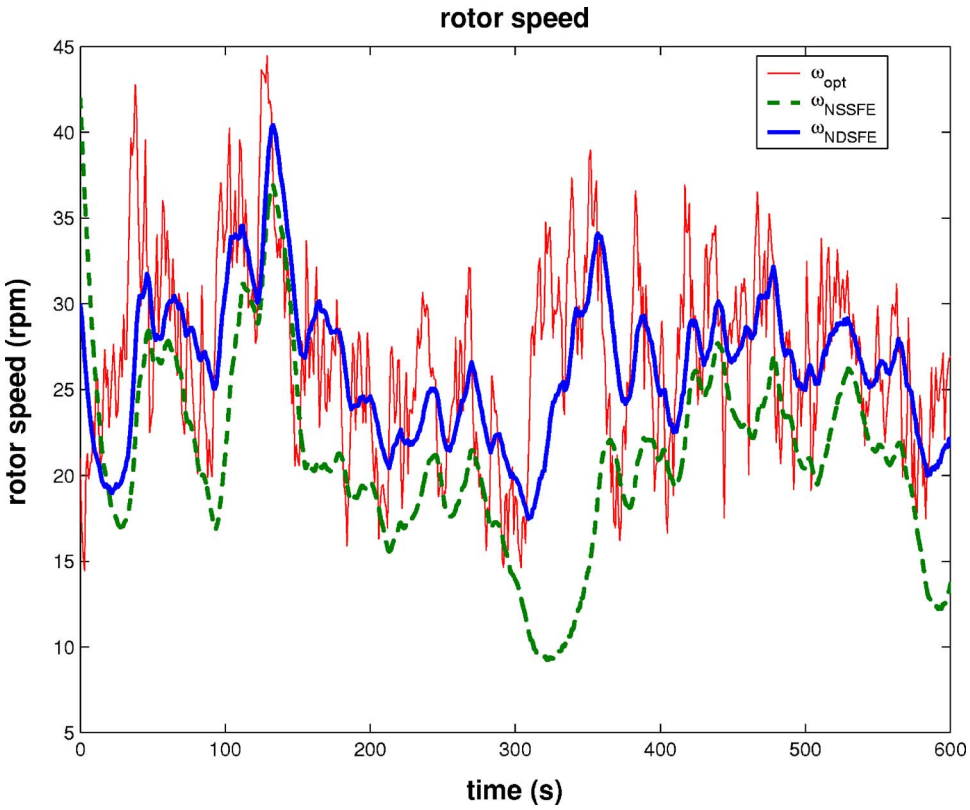

Fig. 11 Nonlinear static and dynamic state feedback controller, with estimator: rotor speed responses with FAST

method approximates an ideal centered white Gaussian noise. The signal-to-noise ratio (SNR) is approximately 7 dB. In addition, a constant, additive disturbance d of 10 kN·m on the control torque T_g has also been introduced. A common phenomenon that can correspond to a constant additive disturbance on the generator torque is the static friction that can be considered as unknown and constant additive torque. For this end, such a disturbance is chosen.

Figure 7(*a*) shows that the rotor speed ω_r tracks the mean tendency of the optimal rotational speed $\omega_{r_{opt}}$ without tracking the turbulent component. The difference between the rotor speed and its optimal reference is most evident during the start-up transient. Figure 8(*a*) shows acceptable control loads where the commanded torque does not exceed the design maximum of 162 kN·m. The generator torque remains smooth and induces low-frequency variations in the generator currents. These are good conditions for electrical devices.

5.2 Validation Using FAST. The nonlinear dynamic state feedback controller was implemented using the FAST wind turbine dynamic simulation. Figure 7(*b*) shows that the rotor speed variations remain smooth while tracking the mean tendency of the optimal rotational speed. Similarly to the mathematical model, the differences between the optimal rotor speed reference and rotor speed occur during the start-up transient. Although the generator torque from the FAST model (Fig. 8(*b*)) is greater than that obtained with the mathematical model, it remains below the maximum acceptable value. One can also observe that the electrical power produced by the simulator output is less than the one produced by the simplified mathematical model (Fig. 9). This decrease can be interpreted by the greatest complexity of the wind turbine simulator that includes more flexible elements and consequently induces more power losses than the simplified mathematical model.

The nonlinear dynamic state feedback controller with estimator (NDSFE) ensures the rejection of the disturbance on the control torque. The Kalman filter used with the Newton algorithm provides a good estimate of the wind speed (Fig. 10) through the aerodynamic torque estimate and rotor speed estimate even with the noisy measurements of ω_r and T_g. Figures 11–13 compare the performance obtained using the nonlinear static and the nonlinear dynamic state feedback controllers. In Fig. 11, the nonlinear static state feedback controller is unable to reject the unknown disturbance applied to the control input. This is the source of the deviation of the rotor speed from its optimal reference between 300 and 400 s. Conversely, the nonlinear dynamic state feedback controller (Fig. 5) succeeded in keeping the rotor speed in the neighborhood of the optimal reference speed in spite of the presence of the disturbance. Figure 12 shows the additional control torque demanded by the NDSFE controller to reject the additive disturbance. The control torque still remains below the upper bound, though. Figure 13 shows that this disturbance rejection results in increased energy capture for the NDSFE controller as compared to the nonlinear static state feedback controller.

These new controllers are compared with the two baseline controllers described in Sec. 2.5. The simulations were conducted with the FAST model with the same operating conditions, disturbance, and measurement noise.

The ATF controller tuning parameter is set to be $K_c=a_0J_t$, with $a_0=0.1$. The constant a_0 of the NSSFE is also fixed to 0.1. The constants b_0, b_1 of the NDSFE are 0.01 and 0.2, respectively. k_{opt} is fixed to 5.38×10^3. The performance differences are illustrated in Fig. 14 and tabulated in Table 2. The power capture efficiency is defined as the ratio between the energy captured during the simulation and the maximum amount of energy available if the turbine could operate at its optimal power coefficient.

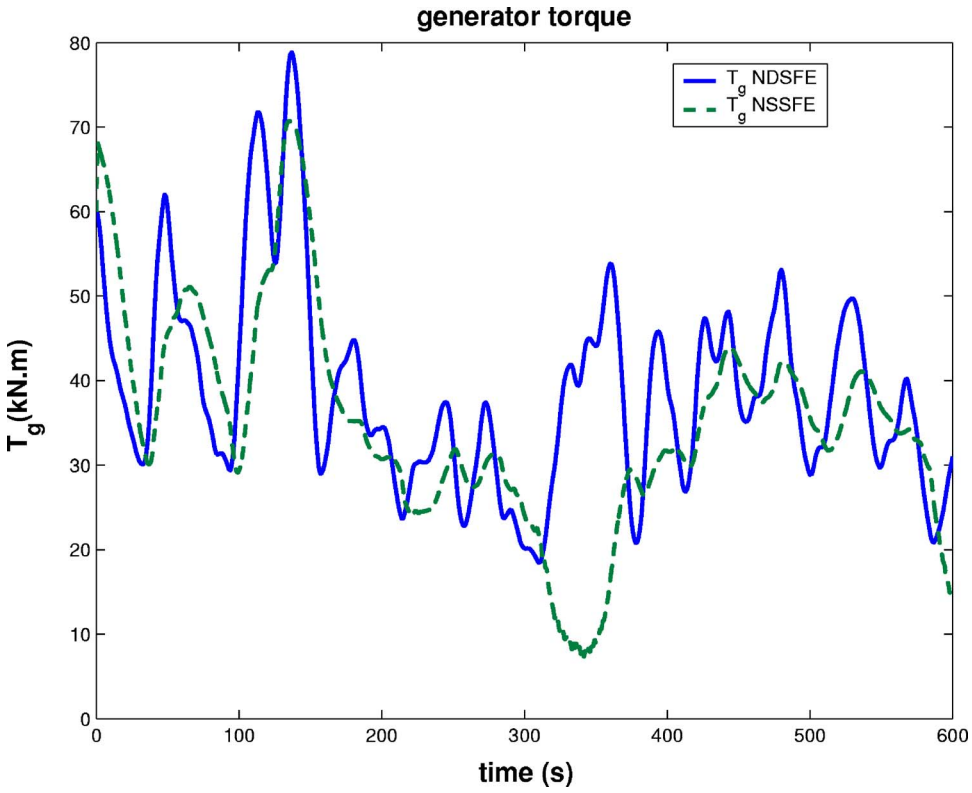

Fig. 12 Nonlinear static and dynamic state feedback controller, with estimator: generator torque responses with FAST

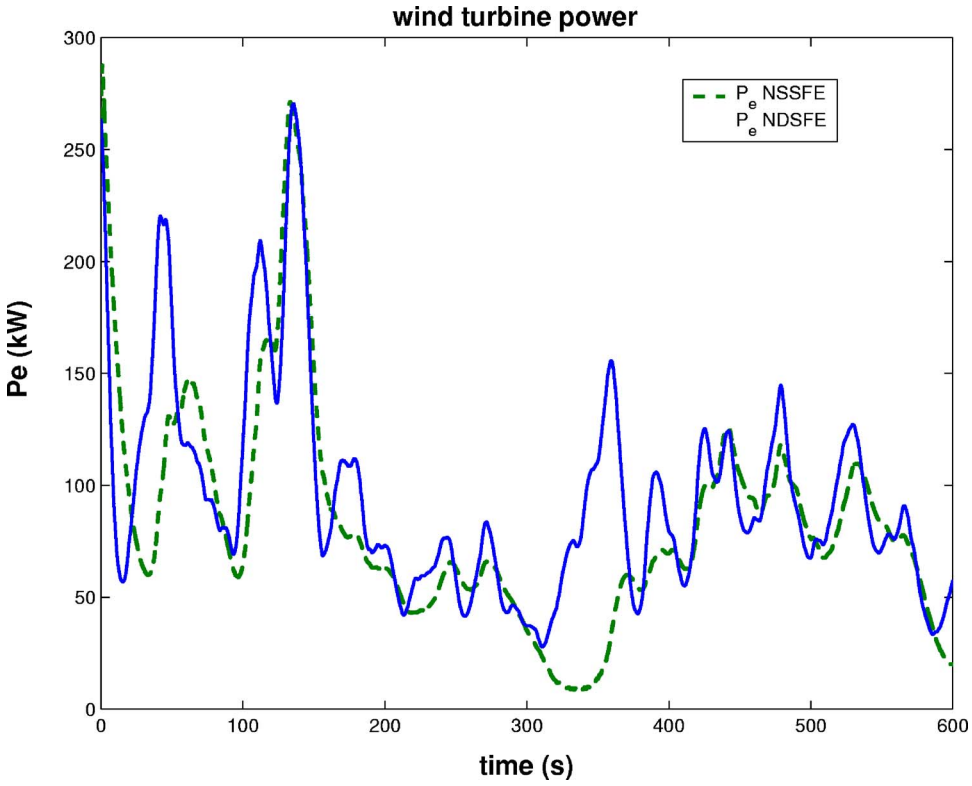

Fig. 13 Nonlinear static and dynamic state feedback controller, with estimator: wind turbine power with FAST

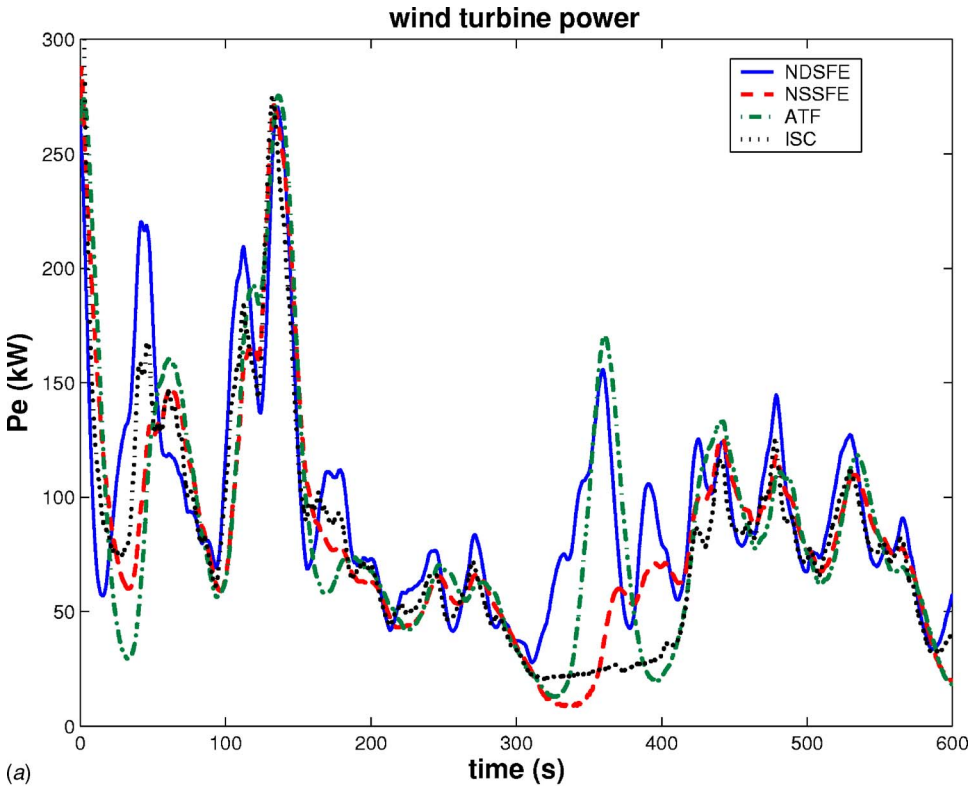

(*a*)

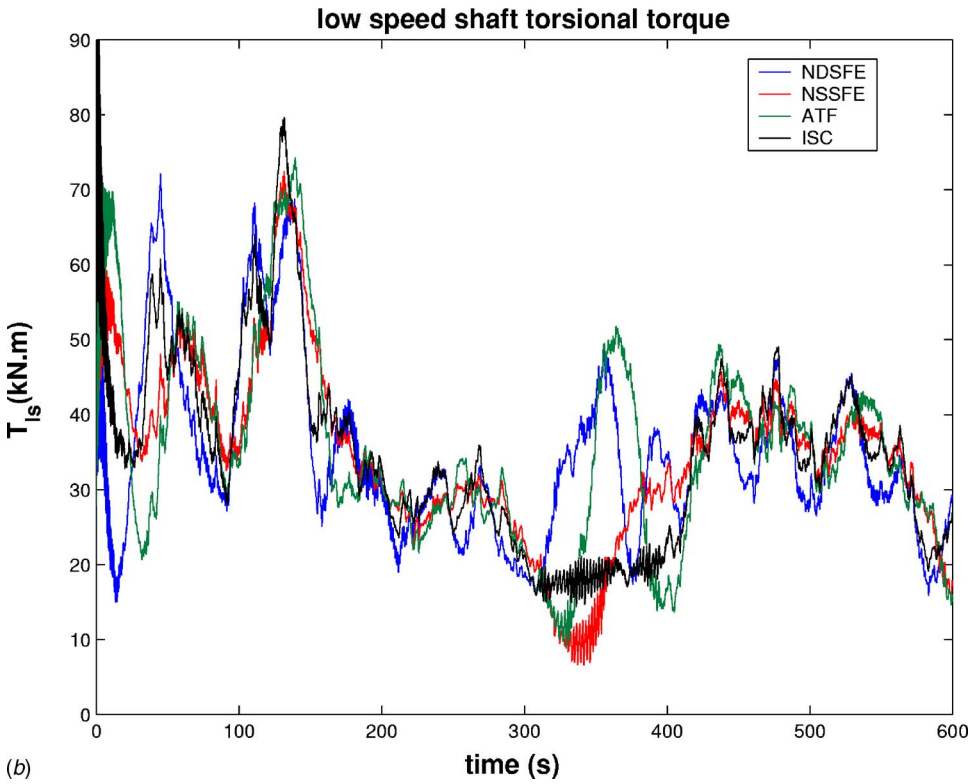

(*b*)

Fig. 14 Electrical power and low speed shaft torque using the different control strategies

$$\text{Efficiency} = \frac{\int_{t_{ini}}^{t_{fin}} P_e \, dt}{\int_{t_{ini}}^{t_{fin}} P_{a_{opt}} \, dt} \tag{34}$$

where

$$P_{a_{opt}} = \frac{1}{2}\rho\pi R^2 C_{p_{opt}} v^3 \tag{35}$$

and P_e is the electrical power.

For simplicity reasons, widely used procedures for fatigue evaluation of gearbox loads rely essentially on the load history of the high speed shaft torque and account only partially for the

Table 2 Comparison of the different control strategies

	Efficiency (%)	T_{hs} standard deviation (kN·m)	max(T_g) (kN·m)
ISC	51.79	12.73	112.34
NSSFE	61.23	11.87	70.70
ATF	63.43	13.19	76.99
NDSFE	69.96	11.59	70.90

three-dimensional character of dynamic drive train loads.

We assumed that this evaluation is sufficient in our case. However, simplified methods like purely torsional models cannot properly reproduce the loads in some elements of the drive train. The dynamic character of certain gearbox loads, such as those on the planet carrier bearings, require detailed dynamic drive train models, which reproduce load frequencies and amplifications of the individual gearbox components with sufficient accuracy. More efficient techniques can then be used to take into consideration the nonlinear and three-dimensional character of wind turbine dynamics; it will be interesting to deduce the load duration distribution [24] and rain flow counts [25] from the global dynamic model, individually for each drive train component. This requirement leads to the use of implicitly coupled analysis techniques like the finite element method and multi-body-system approaches. In that case, the introduction of dynamic load amplitude and load cycle correction factors for different gearbox components and for different load directions might permit us to improve the fatigue calculations [13].

Figure 14(*a*) shows that the produced electric power using the NDSFE controller is greater than that of the other controllers. In the time interval from 300 to 400 s the effect of the disturbance is evident. The ISC, NSSFE, and ATF controllers do not reject the disturbance and therefore power is lost. However, the NDSFE controller does reject the disturbance capturing energy during this period. The low-speed shaft torque oscillations tend to be reduced during this period for the NDSFE controller as shown in Fig. 14(*b*).

The NDSFE controller achieves an 18% increase in efficiency over the ISC controller with a decrease of 1.14 kN·m on the standard deviation of the low-speed shaft torque. The efficiency decrease of the ISC can be justified on the one hand by the presence of a disturbance profile that this controller is not able to reject and on the other hand by the high turbulence of the wind speed that is not taken into account, as this controller is synthetized in steady-state regime.

6 Conclusion

For a variable-speed wind turbine, the primary control objective below rated power is to extract the maximum amount of energy from the wind. The control authority, however, must not exceed design constraints and must not introduce excessive transient loads. Many existing control techniques assume the wind and the turbine operate in steady-state conditions. Consequently, significant power losses occur due to wind speed variability. Controllers based on nonlinear static and dynamic state feedback linearization with asymptotic rotor speed reference tracking were proposed. With the aim of accounting for the wind turbine nonlinear aerodynamic characteristics as well as the stochastic nature of the wind, an aerodynamic torque and wind speed estimator was developed. These controllers were compared to standard controllers using an aeroelastic wind turbine simulator. The nonlinear dynamic state feedback with estimator controller demonstrated the ability to reject a disturbance and operate with measurement noise. In so doing, this controller extracted more power than the other controllers. This study has produced satisfactory results demonstrating the efficiency improvement capability of the new controllers.

Nomenclature

v = wind speed, $\mathrm{m\cdot s^{-1}}$
ρ = air density, $\mathrm{kg\cdot m^3}$
R = rotor radius, m
P_a = aerodynamic power, W
$P_{a_{opt}}$ = optimal aerodynamic power, W
T_a = aerodynamic torque, N·m
λ = tip speed ratio
β = pitch angle, deg
λ_{opt} = optimal tip speed ratio
β_{opt} = optimal pitch angle, deg
C_p = power coefficient
C_q = torque coefficient
ω_r = rotor speed, $\mathrm{rad\cdot s^{-1}}$
ω_g = generator speed, $\mathrm{rad\cdot s^{-1}}$
T_{em} = generator (electromagnetic) torque, N·m
T_g = generator torque in the rotor side, N·m
T_{ls} = low-speed shaft torque, N·m
T_{hs} = high-speed shaft torque, N·m
J_r = rotor inertia, $\mathrm{kg\cdot m^2}$
J_g = generator inertia, $\mathrm{kg\cdot m^2}$
J_t = turbine total inertia, $\mathrm{kg\cdot m^2}$
K_r = rotor external damping, $\mathrm{N\cdot m\cdot rad^{-1}\cdot s}$
K_g = generator external damping, $\mathrm{N\cdot m\cdot rad^{-1}\cdot s}$
K_t = turbine total external damping, $\mathrm{N\cdot m\cdot rad^{-1}\cdot s}$
K_{ls} = low-speed shaft damping, $\mathrm{N\cdot m\cdot rad^{-1}\cdot s}$
B_{ls} = low-speed shaft stiffness, $\mathrm{N\cdot m\cdot rad^{-1}}$
n_g = gearbox ratio
P_a = aerodynamic power, W
P_e = electrical power, W

Appendix: Wind Speed Estimation Algorithm

For instant t, the effective wind speed estimate $\hat{v}(t)$ is obtained using a Newton algorithm from the aerodynamic torque $\hat{T}_a(t)$ and rotor speed $\hat{\omega}_r$ estimates given by the Kalman filter described in Sec. 3.

The iterative form of the algorithm is given by

1. $v_0=\hat{v}(t-T_s)$
2. $\bar{v}_{n+1}=\bar{v}_n-H_n^{-1}g_n$
3. $n:=n+1$
4. stop if $n>n_{\max}$ or $|\bar{v}_n-\bar{v}(n-1)|\big/\bar{v}_n<\varepsilon_{\min}$ else goto 2
5. $n_f:=n;\quad \hat{v}(t)=\bar{v}_{n_f}$

where $\bar{v}_n$ is the result of the first n iterations, and T_s is the sampling rate fixed here to 1 s.

g_n and H_n are obtained by the following expressions:

$$g_n = I(t,v)\big|_{\bar{v}_n} = \hat{T}_a(t) - \frac{1}{2}\rho\pi R^3 C_q(\bar{\lambda}_n)\bar{v}_n^2 \tag{A1}$$

$$H_n = -\rho\pi R^3 C_q(\bar{\lambda}_n)\bar{v}_n + \frac{1}{2}\rho\pi R^4\hat{\omega}_t\frac{\partial C_q(\bar{\lambda}_n)}{\partial\lambda} \tag{A2}$$

with

$$\bar{\lambda}_n = \frac{\hat{\omega}_t R}{\bar{v}_n}.$$

References

[1] Burton, T., Sharpe, D., Jenkins, N., and Bossanyi, E., 2001, *Wind Energy Handbook*, Wiley, New York.

[2] Boukhezzar, B., and Siguerdidjane, H., 2004, "Robust Multiobjective Control of a Variable Speed Wind Turbine," *European Wind Energy Conference Proceedings*, EWEA, London.
[3] Abdin, E. S., and Xu, W., 2000, "Control Design and Dynamic Performance Analysis of a Wind Turbine-Induction Generator Unit," IEEE Trans. Energy Convers., **15**(1), pp. 91–96.
[4] Ekelund, T., 1997, "Modeling and Linear Quadratic Optimal Control of Wind Turbines," Ph.D. thesis, Chalmers University of Technology, Sweden.
[5] Connor, B., Leithead, W. E., and Grimble, M., 1994, "LQG Control of a Constant Speed Horizontal Axis Wind Turbine," *Proceedings of the Third IEEE Conference on Control Applications*, Glasgow, Scotland, August 24–26, Vol. 1, pp. 251–252.
[6] Bongers, P., 1994, "Modeling and Identification of Flexible Wind Turbines and a Factorizational Approach to Robust Control," Ph.D. thesis, Delft University of Technology, Netherlands.
[7] Connor, D., Iyer, S. N., Leithead, W. E., and Grimble, M. J., 1992, "Control of Horizontal Axis Wind Turbine Using H_∞ Control," *Proceedings of the First IEEE Conference on Control Applications*, Dayton, OH, September 13–16.
[8] Battista, H. D., Mantz, R. J., and Christiansen, C. F., 2000, "Dynamical Sliding Mode Power Control of Wind Driven Induction Generators," IEEE Trans. Energy Convers., **15**(14), pp. 451–457.
[9] Song, Y. D., Dhinakaran, B., and Bao, X. Y., 2000, "Variable Speed Control of Wind Turbines Using Nonlinear and Adaptive Algorithms," J. Wind. Eng. Ind. Aerodyn., **85**, pp. 293–308.
[10] van Engelen, T. G., and van der Hooft, E. L., 2005, "Individual Pitch Control - Inventory," ECN Report No. ECN-C–03-138, ECN Windenergie, Petten, The Netherlands, June.
[11] Larsen, T. J., Madsen, H., and Thomsen, K., 2005, "Fatigue Load Computation of Wind Turbine Gearboxes by Coupled Structural, Mechanism and Aerodynamic Analysis," Wind Energy, **8**, pp. 67–80.
[12] Buhl, M. L., 2004, "WT_PERF USER'S GUIDE," Tech. Report, National Renewable Energy Laboratory, Golden, CO.
[13] Heege, A., Radovcic, Y., and Betran, J., 2006, "Fatigue Load Computation of Wind Turbine Gearboxes by Coupled Structural, Mechanism and Aerodynamic Analysis," DEWI Magazin Nr., **28**, pp. 61–68.
[14] Vihriälä, H., Perälä, R., Mäkilä, P., and Söderlund, L., 2001, "A Gearless Wind Power Drive: Part 2: Performance of Control System," *Proceedings of the European Wind Energy Conference*, Copenhagen, Denmark, July 2–6.
[15] Johnson, K. E., 2004, "Adaptive Torque Control of Variable Speed Wind Turbines," NREL Report No. NREL/TP-500-36265, National Renewable Energy Laboratory, Golden, CO, August.
[16] Leithead, W. E., and Connor, D., 2000, "Control of Variable Speed Wind Turbines: Design Task," Int. J. Control, **73**, pp. 1173–1188.
[17] Pierce, K., 1999, "Control Method for Improved Energy Capture Below Rated Power," *Proceedings of the 3rd ASME/JSME Joint Fluids Engineering Conference*, San Francisco, California, July 18–23.
[18] Ma, X., 1997, "Adaptive Extremum Control and Wind Turbine Control," Ph.D. thesis, Danemark, May.
[19] van der Hooft, E. L., Schaak, P., and van Engelen, T. G., 2003, "Wind Turbine Control Algorithms," ECN Windenergie Report, December.
[20] Anderson, B. D. O., and Moore, J. B., 1990, *Optimal Control*, Prentice-Hall, Englewood Cliffs, NJ.
[21] Nijmeijer, H., and Schaft, A. V. D., 1990, *Nonlinear Dynamical Control Systems*, Springer-Verlag, New York.
[22] Boukhezzar, B., and Siguerdidjane, H., 2004, "Robust Nonlinear Control of a Variable Speed Wind Turbine," 8th World Renewable Energy Congress, Denver, CO.
[23] Fingersh, L. J., and Johnson, K., 2002, "Controls Advanced Research Turbine (CART) Commissioning and Baseline Data Collection," NREL Report No. TP-500-32879, National Renewable Energy Laboratory, Golden, CO, October.
[24] "Recommendation to Comply With the Technical Criteria of the Danish Wind Turbine Certification Scheme: Gearboxes," Energistyrelsen, The Danish Energy Authority, RisøNational Laboratory, Roskilde, Danemark, August 2005.
[25] Sutherland, H., and Burwinkle, D., 1995, "The Spectral Content of the Torque Loads on a Turbine Gear Tooth," Wind Energy – 1995, Musial, Hock & Berg, eds., SED Vol. 16, ASME, January–February, pp. 91–97.